Refractive indices of $Sn_2P_2S_6$ at visible and infrared wavelengths

D. Haertle, A. Guarino, J. Hajfler, G. Montemezzani*, P. Günter

Nonlinear Optics Laboratory, Institute of Quantum Electronics, Swiss Federal Institute of Technology, ETH Hönggerberg, CH-8093 Zürich (Switzerland)

* *Present address: Laboratoire Matériaux Optiques, Photonique et Systèmes (MOPS), Université de Metz et Supélec, 2 rue E. Belin, F - 57070 Metz Cedex*

dhaertle@phys.ethz.ch

http://www.nlo.ethz.ch

Abstract: We report on the refractive indices of $Sn_2P_2S_6$ crystals in the wavelength range $550-2300$ nm. The measurements are performed at room temperature using the minimum deviation method. The dispersion is described by a two oscillator model yielding the oscillator energies and strengths (Sellmeier parameters) for all polarization directions. The rotation of the indicatrix in the mirror plane and the direction of the optical axes have also been determined in the wavelength range $\lambda = 550-2200$ nm.

OCIS codes: (120.5710) Refraction; (160.5320) Photorefractive materials

References and links

1. A. Anema, A. Grabar, and T. Rasing, "The nonlinear optical properties of $Sn_2P_2S_6$," Ferroelectrics **183**(1-4), 181–3 (1996).
2. D. Haertle, G. Caimi, A. Haldi, G. Montemezzani, P. Günter, A. A. Grabar, I. M. Stoika, and Y. M. Vysochanskii, "Electro-optical properties of $Sn_2P_2S_6$," Opt. Commun. **215**(4-6), 333–43 (2003).
3. S. G. Odoulov, A. N. Shumelyuk, U. Hellwig, R. A. Rupp, A. A. Grabar, and I. M. Stoyka, "Photorefraction in tin hypothiodiphosphate in the near infrared," J. Opt. Soc. Am. B **13**(10), 2352–60 (1996).
4. A. A. Grabar, I. V. Kedyk, M. I. Gurzan, I. M. Stoika, A. A. Molnar, and Y. M. Vysochanskii, "Enhanced photorefractive properties of modified $Sn_2P_2S_6$," Opt. Commun. **188**(1-4), 187–94 (2001).
5. S. Maerten, N. Dubreuil, G. Pauliat, G. Roosen, D. Rytz, and T. Salva, "Laser diode made single-mode by a self-adaptive photorefractive filter," Opt. Commun. **208**(1-3), 183–9 (2002).
6. M. Jazbinsek, G. Montemezzani, P. Gunter, A. A. Grabar, I. M. Stoika, and Y. M. Vysochanskii, "Fast near-infrared self-pumped phase conjugation with photorefractive $Sn_2P_2S_6$," J. Opt. Soc. Am. B **20**(6), 1241–6 (2003).
7. M. I. Gurzan, A. P. Buturlakin, V. S. Gerasimenko, N. F. Korde, and V. Y. Slivka, "Optical properties of $Sn_2P_2S_6$ crystals," Soviet Physics Solid State **19**(10), 1794–5 (1977).
8. Y. M. Vysochanskii and V. Y. Slivka, *Ferrolelectrics of $Sn_2P_2S_6$ Family. Properties in Vicinity of Lifshitz Point (in Russian)*, p. 264 (Oriana-Nova, 1994).
9. A. A. Grabar, Y. M. Vysochanskii, S. I. Perechinskii, L. A. Salo, M. I. Gurzan, and V. Y. Slivka, "Thermooptic investigations of ferroelectric $Sn_2P_2S_6$," Soviet Physics Solid State **26**(11), 2087–9 (1984).
10. C. D. Carpentier and R. Nitsche, "Vapour growth and crystal data of the thio(seleno)-hypodiphosphates $Sn_2P_2S_6$, $Sn_2P_2Se_6$, $Pb_2P_2S_6$, $Pb_2P_2Se_6$ and their mixed crystals," Materials Research Bulletin **9**(4), 401–10 (1974).
11. R. Nitsche and P. Wild, "Crystal growth of metal-phosphorus-sulfur compounds by vapor transport," Materials Research Bulletin **5**(6), 419–23 (1970).
12. G. Dittmar and H. Schäfer, "Die Struktur des Di-Zinn-Hexathiohypo-diphosphats $Sn_2P_2S_6$," Zeitschrift fuer Naturforschung **29B**(5-6), 312–7 (1974).
13. *ANSI/IEEE Std 176 - IEEE Standard on Piezoelectricity*, p. 242 (IEEE, Inc; 345 East 47th Street, New York, NY 10017, USA, 1987).
14. E. Hecht, *Optics*, pp. 297–299 (Addison-Wesley World Student Series Edition, Reading, UK, 1987).

#5848 - $15.00 US Received 24 November 2004; revised 7 March 2005; accepted 8 March 2005

15. K. Kuepper, B. Schneider, V. Caciuc, M. Neumann, A. V. Postnikov, A. Ruediger, A. A. Grabar, and Y. M. Vysochanskii, "Electronic structure of $Sn_2P_2S_6$," Physical Review B **67**(11), 115,101–1 (2003).
16. A. A. Lavrentyev, B. V. Gabrelian, I. Y. Nikifororv, J. J. Rehr, and A. L. Ankudinov, "Electronic structure and chemical bonding of phosphorus contained sulfides $InPS_4$, Tl_3PS_4, and $Sn_2P_2S_6$," J. Phys. Chem. Solids **64**(12), 2479–2486 (2003).
17. S. H. Wemple and M. DiDomenico, Jr., *Electrooptical and nonlinear optical properties of crystals*, vol. 3, p. 264 (Academic Press, New York (R. Wolfe ed.), 1972).
18. M. DiDomenico, Jr. and S. H. Wemple, "Oxygen-octahedra ferroelectrics. I. theory of electro-optical and nonlinear optical effects," J. Appl. Phys. **40**(2), 720–34 (1969).
19. B. K. Tanner, *X-ray diffraction topography* (Oxford a.o.: Pergamon Press, 1976).
20. H. A. Haus, *Waves and fields in optoelectronics*, pp. 307–309 (Prentice-Hall, Inc. Englewood Cliffs, NJ 07632, 1984).

1. Introduction

Tin thiohypodiphosphate ($Sn_2P_2S_6$) is a wide bandgap semiconductor ferroelectric with interesting nonlinear optical properties [1] and large electro-optical coefficients [2]. In addition it is also a very attractive photorefractive material showing fast photorefractive grating recording times and large refractive index change in the red and near infrared spectral region [3, 4]. These properties make $Sn_2P_2S_6$ an interesting material for several applications where laser diodes are employed (laser stabilization [5], beam cleanup, optical phase conjugation [6]). The wide optical transparency range extending from $\lambda = 0.53$ μm to $\lambda = 8$ μm [7] also allows optical parametric generation of infrared wavelengths not accessible with standard nonlinear optical crystals.

For the prediction of the phase-matching conditions, the principal refractive indices and the orientation of the indicatrix in the *xz*-plane have to be known with a reasonable accuracy. Complete and sufficiently accurate data for $Sn_2P_2S_6$ are not available in the literature. Preliminary refractive indices at room temperature for the visible and near-IR spectral range are given in [8], but no data for some spectral regions (e. g. from 650 to 1300 nm) is given. In addition the accuracy of these data is two orders of magnitude lower than the results reported here. Ref. [9] gives the temperature dependence of the refractive indices at $\lambda = 633$ nm and the relative rotation of the indicatrix between $\lambda = 510 - 810$ nm. The absolute position of the indicatrix has been reported in [2].

In this paper measurements of the refractive indices at 295 K in the wavelength range $550 - 2300$ nm are presented. The absolute accuracy of the measurements is better than $2 \cdot 10^{-4}$. The dispersion of the data is analyzed and described with a two-oscillator Sellmeier model.

In $Sn_2P_2S_6$ the indicatrix has a rotational degree of freedom in the mirror plane of the crystal (*xz*-plane). Its angle to the *x*-axis is measured for the wavelength range $\lambda = 550 - 2200$ nm with an accuracy of 0.4°. Phase-matching conditions can be accurately predicted.

2. Crystallographic properties

$Sn_2P_2S_6$ is a proper ferroelectric with monoclinic point group symmetry *m* at room temperature. The crystal undergoes a second-order phase transition to the centrosymmetric paraelectric phase (point group *2/m*) at the temperature $T_C = 338$ K [10].

Optical quality $Sn_2P_2S_6$ single crystals were produced by the conventional vapor-transport technique [10, 11] using iodine as a transporter. We used nominally pure samples exhibiting low photorefractive effects.

In this work we refer to the unit cell chosen by Dittmar and Schäfer [12] and the Cartesian coordinate system according to the IEEE standard on piezoelectricity [13], with $y \parallel b$ perpendicular to the mirror plane, $z \parallel c$, the positive direction of the *x*-axis and the *z*-axis so that the piezoelectric coefficients d_{xxx} and d_{zzz} are positive and $+y$ is chosen so that *xyz* is a right-handed

#5848 - $15.00 US Received 24 November 2004; revised 7 March 2005; accepted 8 March 2005

system. In this system $\mathbf{P}_S \cdot \hat{\mathbf{x}} > 0$ and $\mathbf{P}_S \cdot \hat{\mathbf{z}} < 0$, with $\hat{\mathbf{x}}$ and $\hat{\mathbf{z}}$ the unit vectors in x and z-direction, as we determined by measuring the pyroelectric current.

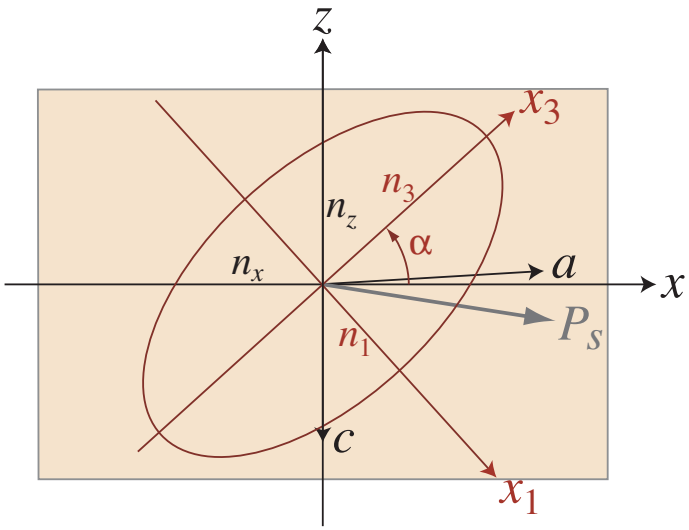

Fig. 1. Position of the indicatrix and spontaneous polarization P_S in the xz-plane at room temperature. This is the mirror plane, perpendicular to b and y. (a,b,c) is the crystallographic system (non-orthogonal for monocline crystals), (x,y,z) is the Cartesian coordinate system, and (x_1,x_2,x_3) is the dielectric coordinate system.

3. Rotation of the indicatrix

In both the paraelectric and ferroelectric phases the indicatrix of $Sn_2P_2S_6$ lies in the mirror plane xz and is rotated by an angle α from the x-axis to its major axis (see Fig. 1).

This rotation angle was measured by determining the rotation angle of the crystal for perfect extinction between crossed polarizers. The crystal was rotated about the y-axis, which coincided with the beam direction.

For $\lambda = 632.8\,\text{nm}$ and $295\,\text{K}$ one gets an angle of either $\alpha = 43.3 \pm 0.4^\circ$ or $\alpha = -46.7 \pm 0.4^\circ$. This is because the measurement cannot distinguish between the major or the minor dielectric axis. We established that the angle between the major dielectric axis and the x-axis is $\alpha = 43.3 \pm 0.4^\circ$ by exploiting the fact that the reflection angle at an internal reflection depends on the rotation of the indicatrix. This to our best knowledge new method is described in Appendix A, and can be used for an easy determination of the $+z$-axis.

For the measurement of the indicatrix rotation we used two rectangular samples with dimensions $5.21 \times 7.58 \times 5.83\ \text{mm}^3$ and $5.07 \times 5.38 \times 4.85\,\text{mm}^3$ along x, y and z axes respectively and polished faces perpendicular to the y-axis. The orientation of the crystallographic axes of these samples was ± 6' as determined by Laue scattering.

The measurements of α were performed using a Perkins Elmer $\lambda 9$ spectrometer as light source and detector. This permitted to automatically scan over the wavelength range of $550 \ldots 2200\,\text{nm}$ for various rotations α_C of the crystal between the two crossed polarizers. We received the complete transmission map as a function of the wavelength λ and the angle α_C, where the minimum represents the index ellipsoid orientation to be determined. For each wavelength the bottom dozen of points was used to fit a parabola and find the minimum. The results

#5848 - $15.00 US Received 24 November 2004; revised 7 March 2005; accepted 8 March 2005

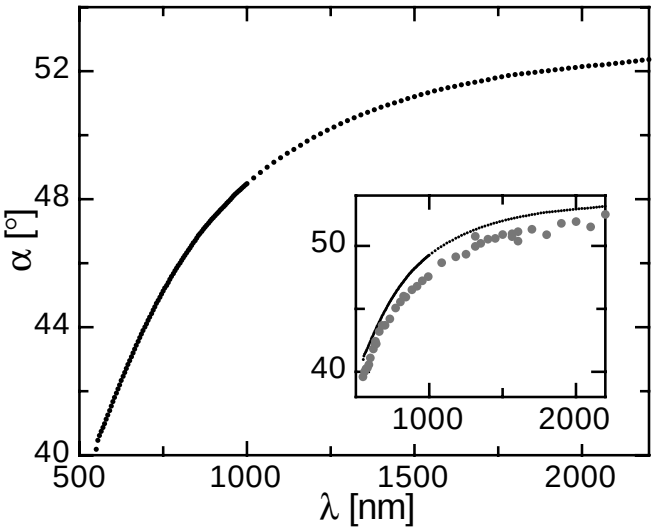

Fig. 2. Measured rotation angle α of the major axis of the indicatrix to the x-axis ($T = 300\,\mathrm{K}$) Error: $\pm 0.4^\circ$. In the inset a comparison is shown with the less precise data calculated from the refractive indices (grey circles).

from one sample are displayed in Fig. 2. The error of $\pm 0.4^\circ$ comes mainly from the uncertainty of the absolute calibration value for α measured at 632.8 nm. The relative error is much smaller (approximately 0.05°).

No model is known to explain the rotation of the indicatrix in low symmetry crystals. However the data in Fig. 2 can be well fitted by the empirical formula (mean absolute deviation $= 1/40^\circ$)

$$\alpha(\lambda) = \alpha_\infty + \frac{\alpha_1}{\lambda^2} + \frac{\alpha_2}{\lambda^4} \tag{1}$$

with $\alpha_\infty = 53.54^\circ$ being the rotation for infinitely long wavelength, $\alpha_1 = -5.523^\circ \mu\mathrm{m}^2$ and $\alpha_2 = 0.4510^\circ \mu\mathrm{m}^4$ (at $T = 300\,\mathrm{K}$).

The temperature dependence of α is given in Ref. [9] and at $T = 295\,\mathrm{K}$ and $\lambda = 633\,\mathrm{nm}$ $\frac{d\alpha}{dt} = -0.16\,\mathrm{K}^{-1}$.

One can also calculate the dispersion $\alpha(\lambda)$ from refractive index measurements of n_1, n_3 and n_z, although this calculation is much less precise than the direct measurement. From our data presented later in this article we get a good agreement with Fig. 2, which is shown in the inset of that figure.

From the principal refractive indices one can also calculate the orientation of the two optical axes of $Sn_2P_2S_6$, i.e. the beam directions, where all polarizations see the same refractive index. In biaxial crystals these beam orientations have to be perpendicular to the middle principal refractive index, $n_{\mathrm{mid}} = n_1$ for $Sn_2P_2S_6$. Both optical axes are off the same angle V from the axis corresponding to the minimum refractive index $n_{\mathrm{min}} (= n_2$ for $Sn_2P_2S_6)$, namely

$$\tan^2 V = \frac{\frac{1}{n_{\mathrm{max}}^2} - \frac{1}{n_{\mathrm{mid}}^2}}{\frac{1}{n_{\mathrm{mid}}^2} - \frac{1}{n_{\mathrm{min}}^2}} \,. \tag{2}$$

The angle $2V$ between the two optical axes is shown in Fig. 3.

#5848 - $15.00 US Received 24 November 2004; revised 7 March 2005; accepted 8 March 2005

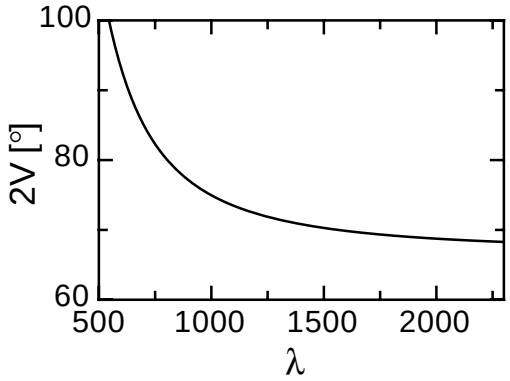

Fig. 3. Angle $2V$ between the optical axes, calculated from the refractive indices given by Eq. (6) and the parameters in Table 3.

4. Refractive index measurement

4.1. Samples

For the measurement of the three principal refractive indices of $Sn_2P_2S_6$ by the minimum deviation method [14] two prisms with different crystallographic orientations are necessary. The orientations must be chosen such that the prism-bisecting plane contains at least one principal axis of the index ellipsoid. We cut two such prisms out of a single crystal and a third prism was cut out of another $Sn_2P_2S_6$ crystal to determine the variations of refractive index between different crystals. The sizes and orientations are given in Table 1. The apex angles φ are approximately 29° and were chosen to be as large as possible (since the error terms $\frac{\partial n}{\partial \varphi}$ and $\frac{\partial n}{\partial \delta}$ diminish with larger apex angles) with the restriction not to let the incidence angle exceed 55°.

Table 1. Size and orientation of the prism samples. Sample 1 and 2 are cut from the same crystal. Both samples 1 and 3 permit to measure n_1 and n_3, while sample 2 permits to measure n_2 and n_z.

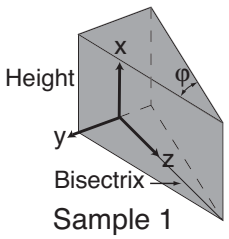

Sample	Bisectrix		Height	
	Length [mm]	Orientation	Length [mm]	Orientation
1	6.0	z	7.5	x
2	6.0	z	4.3	y
3	5.1	z	5.7	x

The non-parallel surfaces are polished to a flatness of $\lambda/4$ of a He-Ne wavelength over the central region of the surfaces. This region has a diameter ranging from 65% to 90% of the crystals edge and is larger than the diameter of the beams used in the experiment. The resulting error in the apex angle due to imperfect centering of the beam on the crystal is approximately 0.001°.

#5848 - $15.00 US Received 24 November 2004; revised 7 March 2005; accepted 8 March 2005

4.2. Experiment

Refractive index measurements were performed at 295 K using the minimum-deviation method. The samples were mounted under a cover and thermally stabilized by a Peltier element to better than ± 0.03 K. The refractive indices were measured at 43 different wavelengths between 550 and 2300 nm. In the visible and near IR region (up to 1181 nm) a xenon spectral lamp was used together with a monochromator. The wavelength passband of this assembly was 1 nm. The absolute setting of the wavelength was checked with laser lines at 632.8 nm and 1313.4 nm. It was found to be better than $\Delta\lambda = 0.5$ nm. The wavelengths above 820 nm corresponded to spectral lines of the xenon lamp. Above 1181 nm an optical parametric amplifier (TOPAS, Light Conversion Ltd) pumped by a 150 fs Ti:Sapphire laser (Clark-MXR) was employed. The wavelength bandpass of this system was several tens of nm, but due to lower dispersion and the geometry of the set-up, measurements with good precision were nevertheless possible. Additional measurements were performed at 632.8 nm with a He-Ne laser, as well as at 1313.4 using a diode pumped YLF laser (ADLAS model DPY 203C, $\Delta\lambda = 0.5$ nm) and at 1565 and 1605 nm with a stabilized diode laser (Santec TSL-220, $\Delta\lambda = 0.005$ nm).

The deflected light was focused on a camera mounted on a rotatable arm controlled by a stepping motor. The rotation stage had a resolution of 0.005 degrees and a positional accuracy of 0.01 degrees. For wavelengths below 950 nm a silicon CCD camera has been used, beyond it a Vidicon camera (Micronviewer 7290A-06E). The cameras were attached to a laser beam analyzer for a precise determination of the position of the peak (more precise than the rotational accuracy). This allowed also the measurement at the central wavelength of the fs-pulse and the accuracy was not limited by its large bandwidth.

The refractive index can be determined by measuring the angle of minimum deviation δ and the apex angle φ of the prism, and using:

$$n = \frac{\sin[(\delta+\varphi)/2]}{\sin(\varphi/2)} \tag{3}$$

The accuracy of the refractive index measurements depends on the accuracy of the angular measurements, temperature, wavelength, and of the orientation of the prism-bisecting plane with respect to the crystallographic axes and is given by:

$$\begin{aligned} \Delta n &= \Delta n_{\mathrm{sys}} + \Delta n_{\mathrm{stat}} \\ &= \frac{\partial n}{\partial \varphi}\Delta\varphi + \frac{\partial n}{\partial \phi_z}\Delta\phi_z + \\ &\quad + \sqrt{\left(\frac{\partial n}{\partial \delta}\Delta\delta\right)^2 + \left(\frac{\partial n}{\partial T}\Delta T\right)^2 + \left(\frac{\partial n}{\partial \varphi_{\mathrm{Fl}}}\Delta\varphi_{\mathrm{Fl}}\right)^2} \\ &< 2.3\cdot 10^{-4} \end{aligned} \tag{4}$$

The apex angle leads to a systematic error Δn_{sys} of the refractive index. We determined the apex angle using a using a Michelson interferometer in which one mirror was substituted by the prism. The statistical accuracy of the apex measurement was 0.001°, giving a contribution of $\frac{\partial n}{\partial \varphi}\Delta\varphi = 7\cdot 10^{-5}$ to Δn. Another systematic error is introduced by the orientational inaccuracy ϕ_z of the principal refractive index axes with respect to the prism-bisecting plane. The orientation of the crystal is controlled by x-ray scattering to 3 arcmin, and the process of fabricating the prisms introduces an error of less than 45 arcmin. For the main refractive indices this gives an error $\frac{\partial n}{\partial \phi_z}\Delta\phi_z < 2\cdot 10^{-5}$. But this error would grow by two orders of magnitude and dominate all others when measuring n_z, since n_z is not extremal in this deviation.

#5848 - $15.00 US Received 24 November 2004; revised 7 March 2005; accepted 8 March 2005

To the systematic error the measurement of the angle of minimum deviation adds a statistical error (Δn_{stat}) with terms given by the inaccuracy of δ, temperature T and flatness of the surfaces of the prisms expressed by an angle φ_{Fl}. The dominant term is due to $\Delta\delta$. Measuring the double minimum deviation angle, $\Delta\delta$ becomes 0.005 degrees and $\frac{\partial n}{\partial \delta}\Delta\delta \approx 1.2\cdot 10^{-4}$. The error caused by the inaccuracy of the temperature depends on the wavelength and polarization. Values of the temperature dispersion are available only at a few wavelengths in the visible [9] and there $\frac{\partial n}{\partial T}\Delta T$ is between $1.7\cdot 10^{-5}$ (for n_2) and $3.6\cdot 10^{-5}$ (for n_1). The last contribution for the inaccuracy Δn_{stat} comes from the imperfect flatness of the prism's surfaces, so that the apex angle changes if the beam comes away from the centric position. In our experiment $\frac{\partial n}{\partial \varphi_{\mathrm{Fl}}}\Delta\varphi_{\mathrm{Fl}}$ ranged from $(1\ldots 7)\cdot 10^{-5}$ depending on the prism used.

The error due to $\Delta\varphi$ grows with larger refractive index, while the one due to $\Delta\delta$ diminishes approximately by the same amount, leading to a total error Δn which is approximately constant over the whole wavelength range.

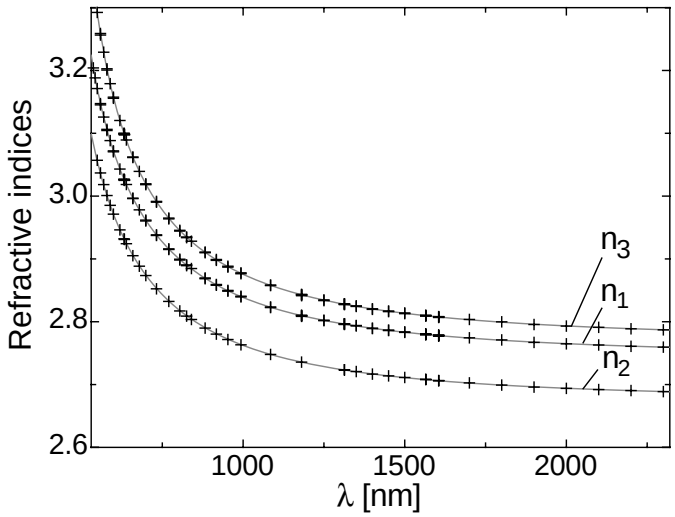

Fig. 4. Principal refractive indices of $Sn_2P_2S_6$ at $T = 295\,\mathrm{K}$ in the wavelength range $550\ldots 2300\,\mathrm{nm}$. The point signs do not correspond to the error bars ($\Delta n \approx 2\cdot 10^{-4}$) and for n_1 and n_3 ($\lambda < 1650\,\mathrm{nm}$) data points from two crystals are displayed. The continuous lines correspond to a two-oscillators Sellmeier model with the parameters given in Table 3.

5. Results

The principal refractive indices of $Sn_2P_2S_6$ at 295 K are shown in Fig. 4. The largest refractive index n_3 reaches 3.3 at $\lambda = 550\,\mathrm{nm}$ close to the absorption edge at 530 nm, while the smallest refractive index n_2 goes down to 2.69 in the infrared.

The measurements give us the lengths n_1, n_2 and n_3 of the principal axes of the indicatrix. As can be seen in Fig. 1, the indicatrix is rotated by the angle α around the *b*-axis with respect to the crystallographic axes. Therefore the refractive indices for light polarization along the Cartesian axes *x*, *y* and *z* are

$$n_x = \left(\frac{\sin^2\alpha}{n_1^2}+\frac{\cos^2\alpha}{n_3^2}\right)^{-\frac{1}{2}}$$

#5848 - $15.00 US Received 24 November 2004; revised 7 March 2005; accepted 8 March 2005

$$n_y = n_2 \qquad (5)$$
$$n_z = \left(\frac{\cos^2\alpha}{n_1^2} + \frac{\sin^2\alpha}{n_3^2}\right)^{-\frac{1}{2}}$$

where α is the angle between the axis x and axis 3 (largest refractive index). Table 2 displays the refractive indices at room temperature for some selected wavelengths.

Table 2. Refractive indices of $Sn_2P_2S_6$ at selected wavelengths ($T = 295\,K$). The values of n_x and n_z are calculated using Eq. (5) and the measured values of n_1, n_3 and α.

λ [μm]	n_1	n_2	n_3	n_x	n_z
0.5500	3.1682	3.0529	3.2887	3.2341	3.2173
0.6328	3.0256	2.9309	3.0982	3.0629	3.0588
0.8080	2.8980	2.8162	2.9438	2.9184	2.9215
0.8600	2.8774	2.7974	2.9199	2.8957	2.8997
1.0640	2.8270	2.7511	2.8623	2.8410	2.8469
1.3134	2.7966	2.7231	2.8282	2.8085	2.8154
1.5500	2.7808	2.7085	2.8107	2.7918	2.7991
2.0000	2.7653	2.6941	2.7935	2.7753	2.7831
2.3000	2.7597	2.6889	2.7873	2.7694	2.7773

The curves of Fig. 4 were obtained by using a two-term Sellmeier oscillator model:

$$n^2(\lambda) - 1 = \frac{S_1\lambda_1^2}{1-(\lambda_1/\lambda)^2} + \frac{S_2\lambda_2^2}{1-(\lambda_2/\lambda)^2}\,, \qquad (6)$$

S_1 and S_2 are the Sellmeier oscillator strengths, λ_1 and λ_2 represent the oscillator wavelengths, and $E_i = \frac{hc}{\lambda_i}$ are its energies. This model, with four adjustable parameters, represents the experimental data of each crystal to within $2\cdot10^{-4}$. Sellmeier expressions with only one oscillator term could not describe the measurements accurately enough. This can be seen graphically in Fig. 5, where we plot $n^2(\lambda)-1$ versus λ^{-2} for the same data as in Fig. 4. A one-oscillator would show a straight line in this figure. The Sellmeier coefficients for the data in Fig. 4 and 5 as well as for calculated values of n_x and n_z are given in Table 3. The main oscillator has an energy E_1 varying between 4.93 and 5.13 eV ($242-252$ nm) depending on the polarization and is $15-22$ times stronger than the weaker oscillator positioned in the violet region ($406-440$ nm). The oscillator energies observed are in accordance with the band structure of $Sn_2P_2S_6$ [15, 16]. Note that $Sn_2P_2S_6$, as most inorganic crystals, obeys to the empirical law of Wemple and DiDomenico [17, 18] that the ratio $E_0/S_0 = (6\pm0.5)\cdot10^{-14}$ eVm^2, where E_0 and S_0 are the oscillator energy and strength in a one-oscillator Sellmeier model.

The optical properties of $Sn_2P_2S_6$, and to an even greater extent the nonlinear optical properties, depend on the growth conditions and may vary from crystal to crystal. To test the reproducibility of the refractive indices we measured n_1 and n_3 in two $Sn_2P_2S_6$ crystals from different bowls (samples nr. 1 and nr. 3). For each crystal and both polarizations the data points lie within a standard deviation $\sigma_{exp} = 3\cdot10^{-4}$ from the corresponding fit. This indicates a good reproducibility even upon a change in polarization. However the refractive indices of sample nr. 3 are approximately $1\cdot10^{-3}$ lower than in sample nr. 1, which is more than the error of the measurement. In order to assess the crystal quality, we performed rocking curve [19] measurements on the two crystals. For sample nr. 1 we measured a FWHM of 36 arcsec for the (400)

#5848 - $15.00 US Received 24 November 2004; revised 7 March 2005; accepted 8 March 2005

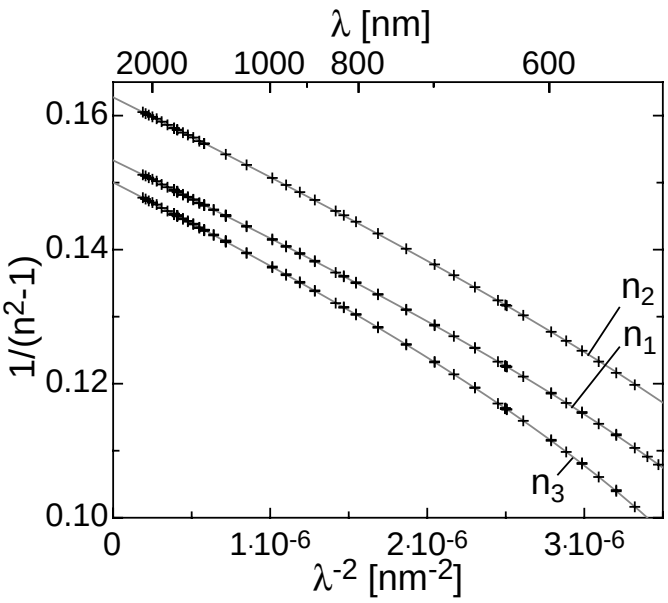

Fig. 5. Principal refractive indices of $Sn_2P_2S_6$ at $T = 295\,\mathrm{K}$ in the wavelength range $550\ldots2300\,\mathrm{nm}$. The coordinate axes are choosen so that a one-oscillator Sellmeier model would appear as a straight line. The continuous lines are from Eq. (6) using the parameters shown in Table 3.

Table 3. Sellmeier coefficients for dispersion of the refractive index of $Sn_2P_2S_6$ at $T = 295\,\mathrm{K}$. The given values are the fit parameters for calculating the refractive indices with (6), while the error is the one of the physical properties.

	$S_1[\mu\mathrm{m}^{-2}]$	λ_1 [nm]	E_1 [eV]	$S_2[\mu\mathrm{m}^{-2}]$	λ_2 [nm]	E_2 [eV]
n_1	93.15 ± 1	251.6 ± 4	4.93 ± 0.08	3.41 ± 1	427.7 ± 7	2.90 ± 0.05
n_2	90.52 ± 1	245.9 ± 6	5.04 ± 0.12	4.06 ± 1	406.5 ± 10	3.05 ± 0.07
n_3	91.51 ± 1	250.4 ± 4	4.95 ± 0.08	4.77 ± 1	440.2 ± 7	2.82 ± 0.05
n_x	94.12 ± 2	242.6 ± 7	5.11 ± 0.14	5.68 ± 1	426.2 ± 9	2.91 ± 0.06
n_z	96.53 ± 2	241.9 ± 7	5.13 ± 0.14	5.45 ± 1	421.6 ± 9	2.94 ± 0.06

peak and 16 arcsec for the (600) one. Sample nr. 3 had FWHMs of 80 and 90 arcsec, respectively. This indicates that both samples have a good crystallographic ordering, but crystal nr. 1 is nearer to the perfect crystalline structure. Since the goal is to measure the refractive indices for the perfect $Sn_2P_2S_6$ structure, and more defects are likely to reduce the refractive indices, we used only the data from sample nr. 1 in this paper. Sample nr. 2, which was used for measuring n_2, was cut from the same bowl as sample nr. 1.

6. Conclusions

Refractive indices, indicatrix rotation and direction of the optical axes of $Sn_2P_2S_6$ have been determined at room temperature. It has been shown that the refractive indices can be well described by a two oscillator Sellmeier equation with a strong UV oscillator ($\lambda_1 = 242 - 252$ nm)

#5848 - $15.00 US Received 24 November 2004; revised 7 March 2005; accepted 8 March 2005

and a weaker oscillator in the violet ($\lambda_2 = 406 - 440$ nm). At 300 K and $\lambda = 550$ nm the major axis of the indicatrix is oriented at an angle $\alpha = 40.2 \pm 0.4^\circ$ off the *x*-axis towards the *z*-axis. This deviation increases with longer wavelengths, reaching an extrapolated angle of 53.5° at infinite wavelength.

Acknowledgments

We thank A. Grabar and Y. Vysochanskii for supplying the crystals and the Swiss National Foundation for the financial support (NF 20-66761.01 and SCOPES 7UKPJ062149). We also thank E. Gini from the FIRST lab (http://www.first.ethz.ch) for the Rocking curve measurements.

Appendix A

We explain here in detail a novel method for determining if the major axis of the indicatrix of $Sn_2P_2S_6$ is rotated by $\alpha = 43.3^\circ$ or $\alpha = -46.7^\circ$ from the *x*-axis, and how it can be used to determine the $+z$ direction.

Let us analyze the beam propagation given in Fig. 6 — where a beam enters a crystal, makes an internal reflection and subsequently exits — for the case that the indicatrix does not lie perpendicular to its surfaces, as happens in monoclinic crystals, or even in uniaxial ones if they are cut obliquely to the optical axis.

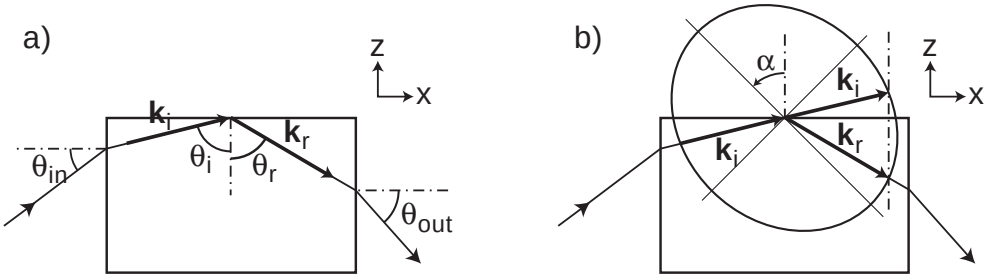

Fig. 6. Schematic of an internal reflection for *p*-polarized light. The outgoing angle θ_{out} is not equal to θ_{in} if the indicatrix is rotated in the *xz*-plane. The energy propagation (Poynting) vector is not parallel to the wave vector **k** in the crystal, but follows it proximately in the case of this figure. In part b) the normal index surface (see text) is drawn. As in Fig. 1, α is the rotation angle of the major axis of the indicatrix from the $+x$-axis, and therefore the rotation angle of the major axis of the normal index surface from the $+z$-axis.

For a polarization that sees the rotation of the indicatrix, i. e. that is in the plane of the rotation, the angle θ_{out} under which the beam leaves the crystal (exit angle), is different from the incidence angle θ_{in}. The difference $\theta_{out} - \theta_{in}$ in $Sn_2P_2S_6$ is approximately 10° for the orientation given in Fig. 6 and changes sign if the crystal is rotated by 180° around *x* or *z*.

For understanding why the angle θ_{out} is not equal to θ_{in}, we assume that the indicatrix is rotated in the *xz*-plane, the crystal is cut along the Cartesian axes, and both the beam propagation and beam polarization are in the *xz*-plane (see Fig. 6). We can then describe the indicatrix by an ellipse rotated by an angle α as defined in Fig. 1. In the **D**-space of the light polarization, the distance between the origin and each point of the indicatrix ellipse corresponds to the refractive index for that polarization direction. In the **k**-space, which is orthogonal to the **D**-space, the indicatrix rotated by 90° (which is called normal index surface [20]) is therefore the refractive index for a given **k** direction.

#5848 - $15.00 US Received 24 November 2004; revised 7 March 2005; accepted 8 March 2005

For a given wavelength, energy conservation forces all the possible wave vectors $\mathbf{k}$ to lie on this normal index surface. At the internal reflection the boundary conditions (translation symmetry in $\mathbf{x}$ direction) imply that

$$\mathbf{k}_i \cdot \mathbf{x} = \mathbf{k}_r \cdot \mathbf{x}$$

so that $\mathbf{k}_r$ is given by the intersection of the normal index surface with a vertical line in Fig. 6b. One sees that the reflection angle θ_r (between the internal reflected wave vector $\mathbf{k}_r$ and the normal to the crystal surface) is not equal to the internal incidence angle θ_i, if the normal index surface (and thus the indicatrix) does not lie perpendicular to the surface.

θ_{out} is larger than θ_{in} if the major axis of the normal index surface is in the II,IV quadrants, so the one of the indicatrix in the I,III quadrants and $0^\circ < \alpha < 90^\circ$. For $90^\circ < \alpha < 180^\circ$, θ_{out} is diminuished, and for certain small incidence angles ($\theta_{\text{in}} < 8^\circ$ and $k_{\text{in},x} < 0$ for $Sn_2P_2S_6$) θ_{out} even becomes negative, i. e. $\mathbf{k}_{\text{out}}$ points up in Fig. 6.

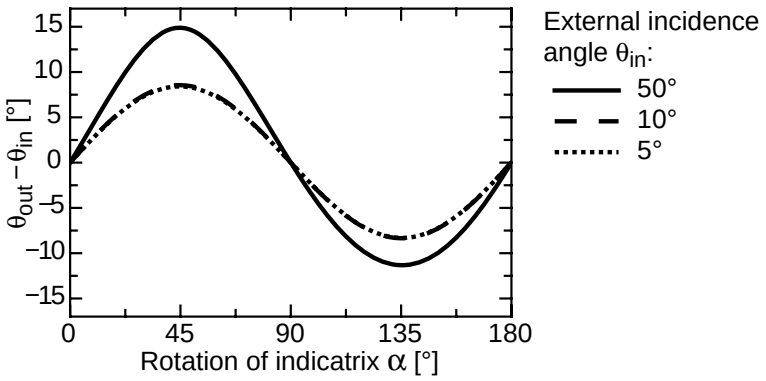

Fig. 7. Calculation of the variation $\theta_{\text{out}} - \theta_{\text{in}}$ versus the rotation of the indicatrix in the xz-plane for $Sn_2P_2S_6$ (Fig. 6).

Figure 7 displays $\theta_{\text{out}} - \theta_{\text{in}}$ versus the rotation angle of the indicatrix for different incidence angles θ_{in}. The change in θ_{out} is maximal at $\alpha = \pm 45^\circ$, while for the indicatrix parallel to the crystal surfaces ($\alpha = 0^\circ,\ 90^\circ,\ 180^\circ$) there is no change. The dependence on θ_{in} is not as strong as on α and does not change the sign of $\theta_{\text{out}} - \theta_{\text{in}}$. For typical main refractive indices n_1 and n_3, the maximum value of $\theta_{\text{out}} - \theta_{\text{in}}$ is nearly constant for $\theta_{\text{in}} < 20^\circ$ and increases for larger θ_{in} due to the sine function in the Snell's law.

In this article we used the effect described here to determine that the major axis of the indicatrix lies in the I,III quadrants of the coordinate system determined by measuring the sign of the piezoelectric coefficients.

We also established that the spontaneous polarization $\mathbf{P}_S$ points in the direction of $+x$. It is now possible to use the internal reflection method to find the $+z$ direction and $\mathbf{P}_S$ for $+x$, which is much easier than the other methods, such as Laue diffraction, the measurement of the sign of the piezoelectric coefficients, the dispersion of the indicatrix rotation α, or, for crystals where α is not near $m \cdot 45^\circ$ ($m \in \mathbf{Z}$), just a precise measurement of α.

#5848 - $15.00 US Received 24 November 2004; revised 7 March 2005; accepted 8 March 2005